TECHNICAL REPORT BRL-TR-3118

BRL

APPLICATION OF A RECHARGEABLE, SMALL CALIBER RAILGUN POWER SUPPLY

ALEXANDER E. ZIELINSKI
KEITH A. JAMISON

JULY 1990

U.S. ARMY LABORATORY COMMAND

BALLISTIC RESEARCH LABORATORY
ABERDEEN PROVING GROUND, MARYLAND

NOTICES

Destroy this report when it is no longer needed. DO NOT return it to the originator.

Additional copies of this report may be obtained from the National Technical Information Service, U.S. Department of Commerce, 5285 Port Royal Road, Springfield, VA 22161.

The findings of this report are not to be construed as an official Department of the Army position, unless so designated by other authorized documents.

The use of trade names or manufacturers' names in this report does not constitute indorsement of any commercial product.

UNCLASSIFIED

REPORT DOCUMENTATION PAGE

Form Approved
OMB No 0704-0188

1. AGENCY USE ONLY (Leave blank)	2. REPORT DATE	3. REPORT TYPE AND DATES COVERED
	July 1990	Final (Jan 89 - Dec 89)

4. TITLE AND SUBTITLE
Application of a Rechargeable, Small Caliber Railgun Power Supply

5. FUNDING NUMBERS
PE: 61221A

6. AUTHOR(S)
Alexander E. Zielinski
Keith A. Jamison

7. PERFORMING ORGANIZATION NAME(S) AND ADDRESS(ES)

8. PERFORMING ORGANIZATION REPORT NUMBER

9. SPONSORING/MONITORING AGENCY NAME(S) AND ADDRESS(ES)
Ballistic Research Laboratory
ATTN: SLCBR-DD-T
Aberdeen Proving Ground, MD 21005-5066

10. SPONSORING/MONITORING AGENCY REPORT NUMBER
BRL-TR-3118

11. SUPPLEMENTARY NOTES
Research sponsored by: Close Combat Armaments Center, SMCAR-CCL-FA, Picatinny Arsenal, NJ 07801-5001

12a. DISTRIBUTION/AVAILABILITY STATEMENT
Approved for public release; distribution unlimited.

12b. DISTRIBUTION CODE

13. ABSTRACT (Maximum 200 words)

A capacitive power supply for driving a railgun load has been developed using solid-state switch gear and electrolytic capacitors. Electrolytic capacitors and solid-state switching devices allow relative ease of component orientation and insensitivity to field conditions. The circuit is constructed such that half the bank capacitance is initially charged while the other half is uncharged. Both halves are connected in series with the load. When the discharge is initiated, the current passing through a railgun simultaneously charges the uncharged section of the capacitor bank. The current waveform is nearly sinusoidal; its half-cycle time may be easily matched to the projectile acceleration time by including a series inductor. Theoretical results and experimental data are presented from a 4 module, 7500 J and 30 kA per module, laboratory setup. This type of supply is ideal for use with augmented and multiturn railguns. In these configurations, the pulse shaping inductance becomes part of the railgun itself. Because the circuit may be timed so that zero current coincides with projectile exit, projectile tip off is reduced and firing becomes flashless. In fact, since the SCRs open when the load current goes to zero, the current zero may precede projectile exit.

14. SUBJECT TERMS	15. NUMBER OF PAGES
Electric Propulsion, Solid Armature, Sliding Contact, Electromagnetics	30
	16. PRICE CODE

17. SECURITY CLASSIFICATION OF REPORT	18. SECURITY CLASSIFICATION OF THIS PAGE	19. SECURITY CLASSIFICATION OF ABSTRACT	20. LIMITATION OF ABSTRACT
Unclassified	Unclassified	Unclassified	UL

UNCLASSIFIED

INTENTIONALLY LEFT BLANK.

TABLE OF CONTENTS

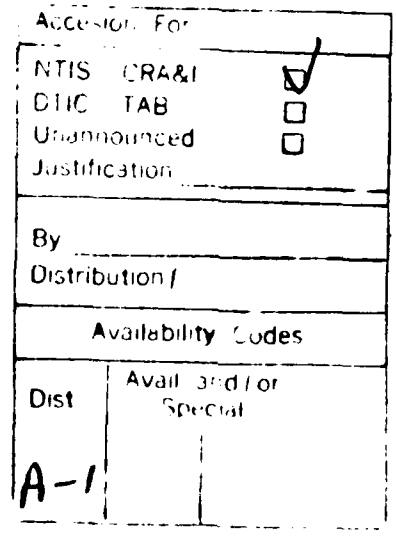

INTENTIONALLY LEFT BLANK.

LIST OF FIGURES

LIST OF TABLES

Intentionally Left Blank.

ACKNOWLEDGMENTS

This work is supported by the Close Combat Armament Center, U. S. Army Armament Research Development and Engineering Center (ARDEC), Picatinny Arsenal, NJ.

The technical and editorial comments of Mr. Henry S. Burden are gratefully acknowledged.

Intentionally Left Blank.

1. INTRODUCTION

Traditionally, the power supply for an electromagnetic launcher (EML) has overshadowed the barrel both in size and weight. When considering laboratory operation, the construction of a demonstration device, or postulating a future weapons system, the power supply usually dominates the planning, costs, and facilitation. Throughout the history of electromagnetic guns, a wide variety of power supplies and power conditioning circuits have been considered. Many variations of generators, alternators, batteries, and flux compressors have been used to provide electrical power for EMLs. Power conditioning is often accomplished with high current circuits comprised of inductors, capacitors, or transformers. These components are actuated with specialized high current switching. Very recently, solid-state switching devices have been manufactured with sufficient current ratings so that small arrays of devices may be used to provide launcher power.

Although the power supply may dominate the planning phases of an EML project, it should not be forgotten that the power conditioning circuit will dictate the performance of the launcher. The shape of the current waveform defines the acceleration profile that the projectile will undergo. The stresses within the launcher are also a direct function of the output of the power circuit. The firing protocol, burst size, and burst rate of fire are, again, parameters which are set not by the launcher but by the power supply. In particular, a small caliber weapon may have a requirement for a very high rate of fire during a burst. Furthermore, the accurate launch of a small projectile will likely require a very small driving force as the projectile leaves the muzzle. The requirements listed above imply a strong correlation between the ultimate mission of an EML and the performance of the power circuit. Even in the early phases of component development, it is valuable to emulate the circuit performance which is desired in the final application.

In this paper we present a concept for a rapid-fire EML power supply. This concept focuses on our need to develop small caliber projectiles. The power conditioning circuit extracts electrical energy from a laboratory outlet and delivers the high current necessary to drive a railgun. The energy is stored in electrolytic capacitors, and the waveform is shaped with additional pulse forming network (PFN) circuit inductance. The power is switched by silicon controlled rectifiers (SCRs).

This report describes the theory of circuit operation as well as the numerical model developed to aid in understanding power supply behavior. Section 4 describes experimental results obtained from a four module supply. Section 5 examines the possibilities of the power supply for consideration as part of a rapid fire weapons system. Finally, conclusions are presented in Section 6.

2. THEORY OF OPERATION

Consider a simple, series LC, ringing discharge circuit. When a discharge is initiated, the energy stored electrostatically in a positively charged capacitor is transferred to magnetic field energy and back to electrostatic energy stored at negative voltage. If the resistance is negligible, the negative maximum voltage should nearly equal the positive maximum voltage. If a railgun were inserted as the load, the losses (i.e., resistive and kinetic) would simply lower the negative voltage at the end of the current half cycle. If the load were removed at this point, charge could be very quickly added to the capacitor to restore the energy needed for a second firing. One drawback with this type of circuit is that the capacitor must be rated to withstand twice the initial potential difference. This restricts the capacitor charge to half of the rated voltage or 25% of the rated stored energy. One way to circumvent this is to use two series capacitors with their negative terminals connected and diodes across each to prevent voltage reversal. The voltage across either capacitor at any point in time is equal to or less than the initial charge voltage. Accordingly, each capacitor is utilized at the rated stored energy, but only half of the capacitors are charged. This type of circuit is shown in Figure 1. The resistive and inductive elements in the circuit will be described in Section 2. Capacitor C_a (positive phase) is initially charged. When the discharge is initiated, current flows from capacitor C_a, through the load, to capacitor C_b (negative phase). The current, I, causes capacitor C_b to charge. If there were no losses, the final recharge voltage on capacitor C_b would equal the initial voltage on capacitor C_a. The final recharge voltage on capacitor C_b, with losses included, will be somewhat lower than the initial voltage on capacitor C_a and must be determined from circuit simulations. Typical measured current and output voltage waveforms for two sequential discharges are shown in Figure 2.

Electrolytic capacitors typically have very large capacitance but are rated at less than 500 V. They therefore need little added series inductance to match the half cycle discharge time to the acceleration time of a railgun projectile. Voltage reversal across their terminals must, however, be prevented. On the whole, electrolytic capacitors are appropriate for powering small railguns. When many kilojoules are required, the capacitance can be on the order of 1/10 F. The series pulse shaping inductance will be on the order of one microhenry, which matches the inductance of multiturn railguns less than one meter long. In addition, operating a pulsed power system at 500 V or less is significantly safer and is less expensive since buying electrolytics in quantity can offer considerable cost savings. Ninety-six 3100 μF, 450 V electrolytic capacitors, unused by another project, were readily available and well suited for this application.

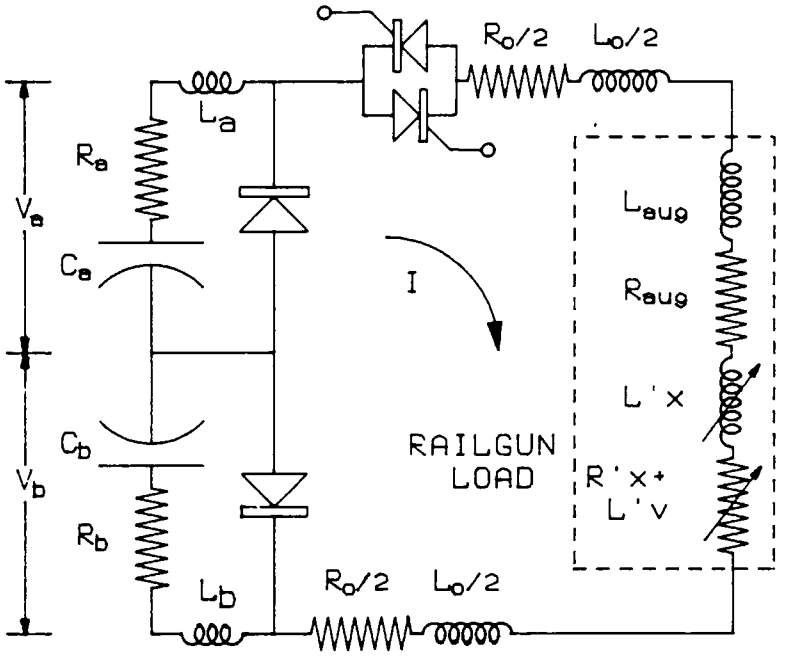

Figure 1. Series Capacitor Power Supply.

Solid-state switching is relatively easy to control. For the power supply considered here, SCRs can be stacked as the switching element. The triggering of the SCR's gates is done using standard pulse forming techniques. A low power, square pulse is applied to the base of a two-stage transistor current amplifier (Darlington pair), which drives the primary of an eight-output pulse transformer. The rise time of the gate pulse is less than one microsecond, a time considered adequate for the expected rate of current rise through the SCRs. The SCR stack is primarily used as a closing switch but will naturally open at a current zero crossing which normally occurs at the half period for a sinusoidal current pulse. The gate pulse is applied to the gates of both the positive and negative phase SCRs regardless of which phase is being discharged. A more elaborate gate pulsing scheme would allow for various combinations of current magnitude and pulse width for driving a railgun armature. The nature of the gate pulsing circuit allows it to be integrated into an all electric system and adapts easily to computer control.

Available stored energy and circuit code simulations determine both the solid-state devices for use in the modules and the load consistent with the configuration of a readily available launcher.

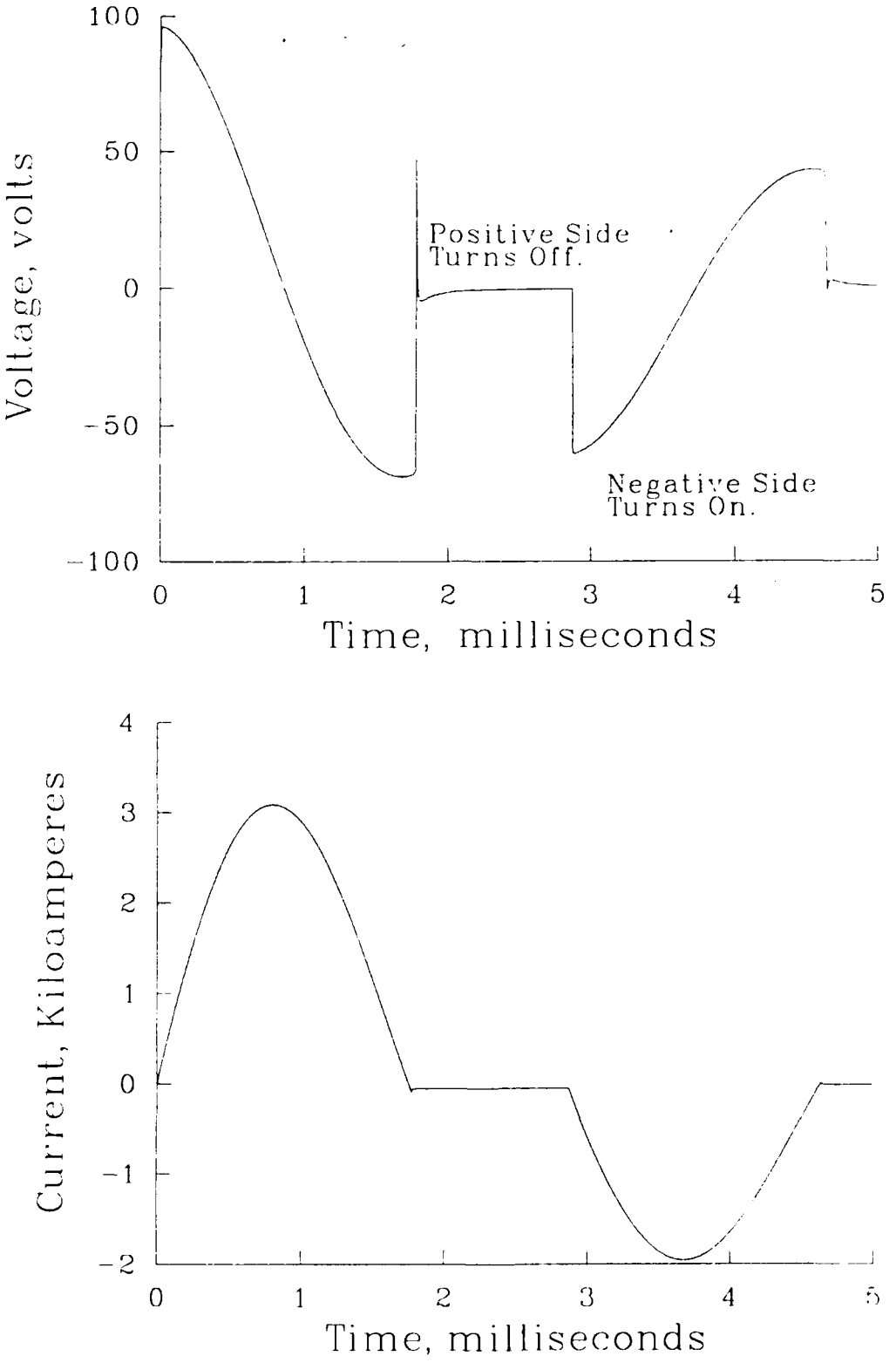

Figure 2. Experimentally Measured Voltage (Top) and Current (Bottom) Pulse Train From the Series Capacitor Circuit of Figure 1.

Lying within these constraints, a 6.35 mm square bore, series-augmented, 585 mm long barrel supported by a structure rated for 150,000 A was selected. The projectile mass used to analyze power supply performance is 3 g. The barrel's augmenting turn inductance, resistance, and inductance gradient were measured using pulsed current techniques. Average values are used in the following circuit analysis simulation. Figure 3 displays a photograph of the assembled launcher while Table 1 summarizes the barrel load parameters. A nominal equivalent series resistance (ESR) of 10 mΩ is used for each electrolytic capacitor. The projectile mass was estimated assuming a mass stabilized, solid armature type (Garner et al. 1989).

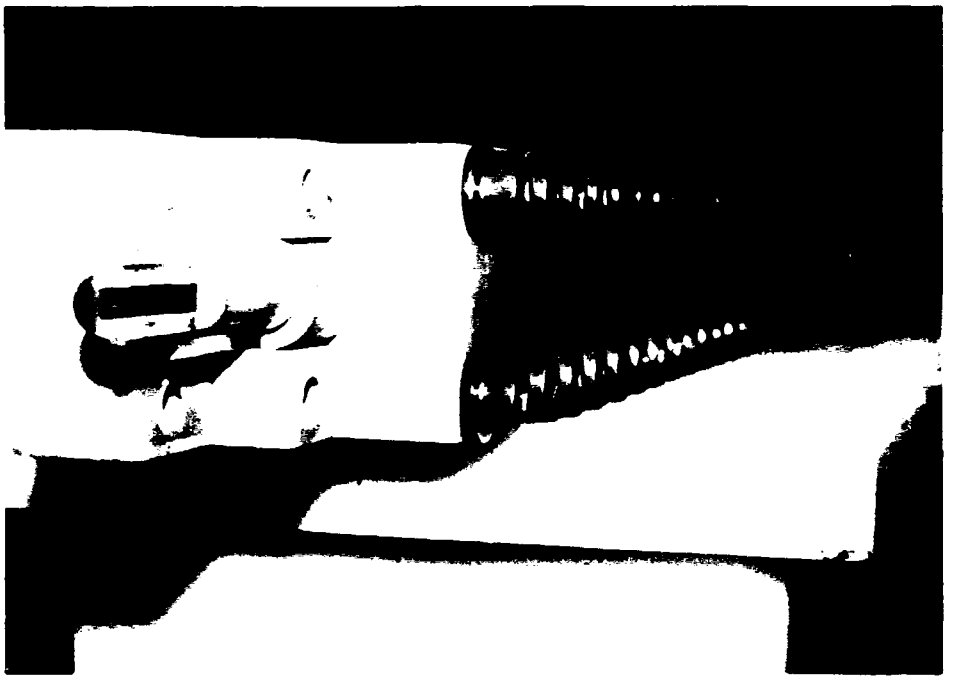

Figure 3. Breech View of the 6.35 mm, Square Bore, Augmented Launcher.

Table 1. BRL Augmented Launcher Parameters.

Bore height (mm)	6.35
Bore width (mm)	6.35
Length (mm)	585.0
Projectile Mass (g)	3.0
Inductance Gradient (μH/m)	0.72
Augmenting Turn Inductance (μH)	0.189

3. CIRCUIT ANALYSIS

The variable elements shown in Figure 1 (L′x and R′x + L′v) correspond to motion-dependent electrical parameters. The position of the projectile and its velocity are denoted by x and v, respectively. The barrel inductance gradient, L′, is easily measured and is nearly independent of armature position. The barrel resistance gradient, R′, is somewhat cumbersome both analytically and experimentally and is calculated as a function of time, assuming constant rail current as:

$$R' = \frac{8}{3h} \sqrt{\frac{4 \mu \rho}{\pi t}}, \tag{1}$$

where h is the bore dimension and μ and ρ are the permeability and resistivity of the rail material (Powell 1988).

From Figure 1, Kirchoff's voltage law can be written as:

$$V_a = I R_{tot} + \frac{di}{dt} L_{tot} - V_b, \tag{2}$$

where

$$R_{tot} = R_a + R_b + L'v + R'x + R_o + R_{aug},$$

and

$$L_{tot} = L'x + L_0 + L_{aug},$$

where L_{aug} and R_{aug} are the augmenting turn inductance and resistance and L_o and R_o are the PFN inductance and resistance, respectively. The resistive component of voltage in equation (2), which accounts for moving a current carrying conductor in a magnetic field, is termed the back electromotive force (EMF) and is represented by the terms IL′v. For initial conditions we assume that capacitor C_a is charged to a voltage V_{cap}, capacitor C_b is uncharged, and all the solid-state devices are assumed to be

ideal. After making the substitution, $di/dt \sim \Delta i/\Delta t$, in equation 2, the relation may be solved for Δi, the increment of current during time, Δt:

$$\Delta i = (V_{cap} - I R_{tot} - V_b) \Delta t / L_{tot}. \quad (3)$$

The values for I, V_{cap}, and V_b may then, by equations (4) through (6), be updated for use in successive iterations:

$$I = I + \Delta i, \quad (4)$$

$$V_{cap} = V_{cap} - (I \Delta t / C_a), \quad (5)$$

and

$$V_b = V_b + (I \Delta t / C_b). \quad (6)$$

The equations for projectile motion which couple the kinematics to the electrodynamics are given by:

$$x = x + v\Delta t, \quad (7)$$

$$v = v + a\Delta t, \quad (8)$$

$$a = F_{tot} / m_p, \quad (9)$$

where a is the acceleration, m_p is the total launch mass, and

$$F_{tot} = 1/2 \quad L'I^2 - F_{air\ drag}. \quad (10)$$

For the simulation, the armature is assumed lossless with no drag between the bore and projectile. However, the reaction of a shock wave driven ahead of the projectile is included and given by:

$$F_{air\ drag} = \frac{(1+\gamma)}{2} h^2 v^2 \rho_0 , \quad (11)$$

where γ is the ratio of the specific heat at constant pressure to that at constant volume (1.4) and ρ_0 is the ambient atmospheric density (1.29 kg/m^3) (Powell 1983). Resistive and inductive circuit parameters employed for the launcher in equation (3) are also iteratively updated from the resulting dynamics by equations (7) and (8). Equations (1) through (11) were assembled into a computer code in order to compare various electrical parameter variations with resulting power supply performance. A first concern in this analysis is the projectile velocity at the muzzle of the barrel. Because of the relatively large number of capacitors available, the power supply can be configured in a number of series/parallel combinations. Table 2 lists the characteristics of three configurations of 48 capacitors making up one of the two, identical phases. The values in column 1 correspond to a configuration with 48 capacitors all in parallel; those in column two, for 24 paralleled groups, each with two capacitors in series; and those in column three, for 16 paralleled groups of three capacitors in series. The bank inductance was considered to be negligible, and any added PFN inductor was assumed to possess a time constant of 5 ms.

Table 2. Capacitor Configurations.

Capacitor Voltage (V)	450	900	1350
$C_a = C_b$ (mF)	148	37.2	16.5
Total ESR, $R_a + R_b$, (mΩ)	0.416	1.67	3.75

Additionally, the amount of PFN inductance needed to tailor the pulse was varied in the code and was done for two cases: with the capacitor equivalent series resistance (ESR) as given in Table 2 and with the ESR assumed to be zero. The PFN inductance for the 450 V and 1350 V cases was varied from 0.1 μh to 1.0 μh, while the 900 V cases had values in the range of 0.25 μh to 1.15 μh. The inductance was incremented by 0.05 μh in all cases. Changing the PFN inductance affects the peak current and pulse width and may be used to obtain the optimum match to the load. In Figure 4, the resulting peak current, which varies with PFN inductance in the configurations simulated, is plotted against the final velocity. The higher values for peak current are obtained at the lower values of PFN inductance. Not plotted is the amount of projectile travel. The configuration which best utilizes the barrel length is the one with the largest capacitance. However, in all cases, the final drive length under electromagnetic acceleration is less than 585 mm. The same optimum capacitor configuration is selected whether the ESR is zero or not, however; a zero ESR would further extend the pulse width and increased projectile drive duration. As the PFN inductance grows, the rail losses, augmenting turn losses, and residual voltage left on the capacitor are all decreased.

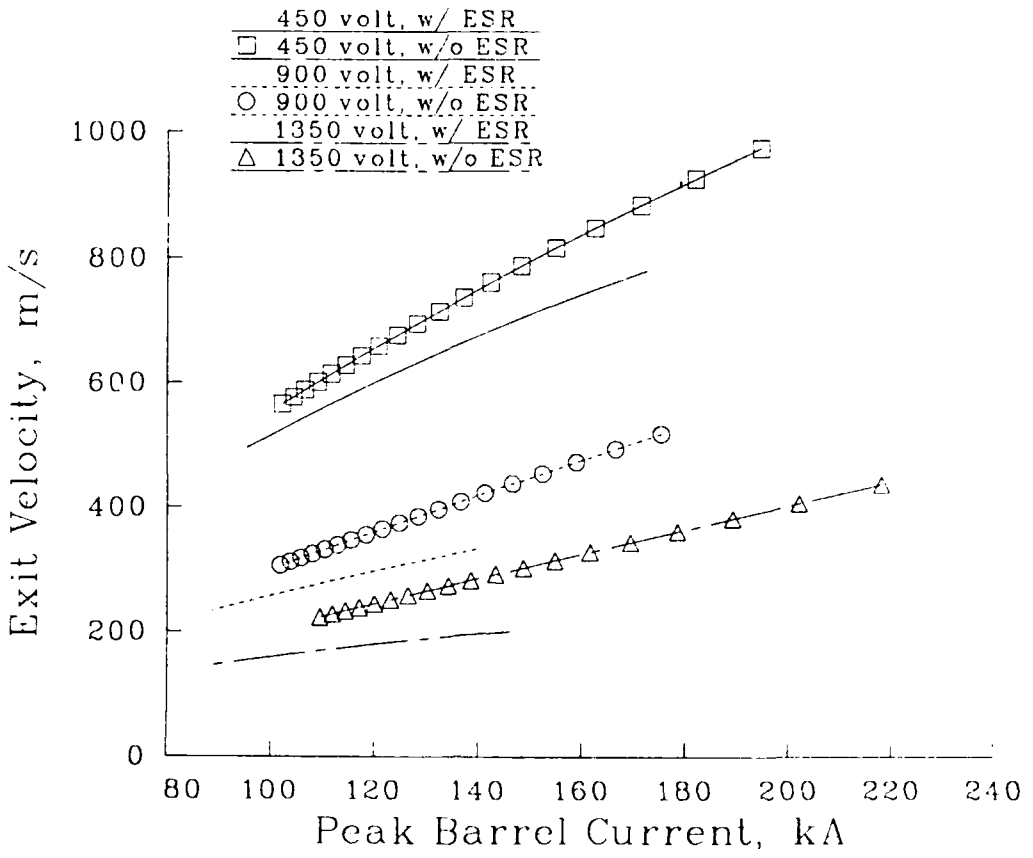

Figure 4. Predicted Velocity vs. Peak Current for Different Capacitor Configurations and PFN Inductance.

A second concern is the recharge voltage on capacitor C_b. The larger the energy transferred to the projectile, the smaller the energy that is transferred to the uncharged capacitor C_b and, consequently, the greater the time to fully recharge capacitor C_b with a current limited recharge supply Thus, for a charging supply of given current capacity, projectile performance will always be bought at the expense of repetition rate. In Figure 5, the recharge voltage (V_b) is plotted against the final velocity for the 450 V capacitor configuration. Both values for capacitor ESR are shown. If the peak power level for the charging supply is known, the recharge voltage axis in Figure 5 can easily be transformed to fire rate. The resultant energy distribution for a total PFN inductance of 0.25 μH with the 450 V capacitor configuration is shown in Figure 6. Relatively little gain in projectile performance is obtained from any further decrease in PFN inductance.

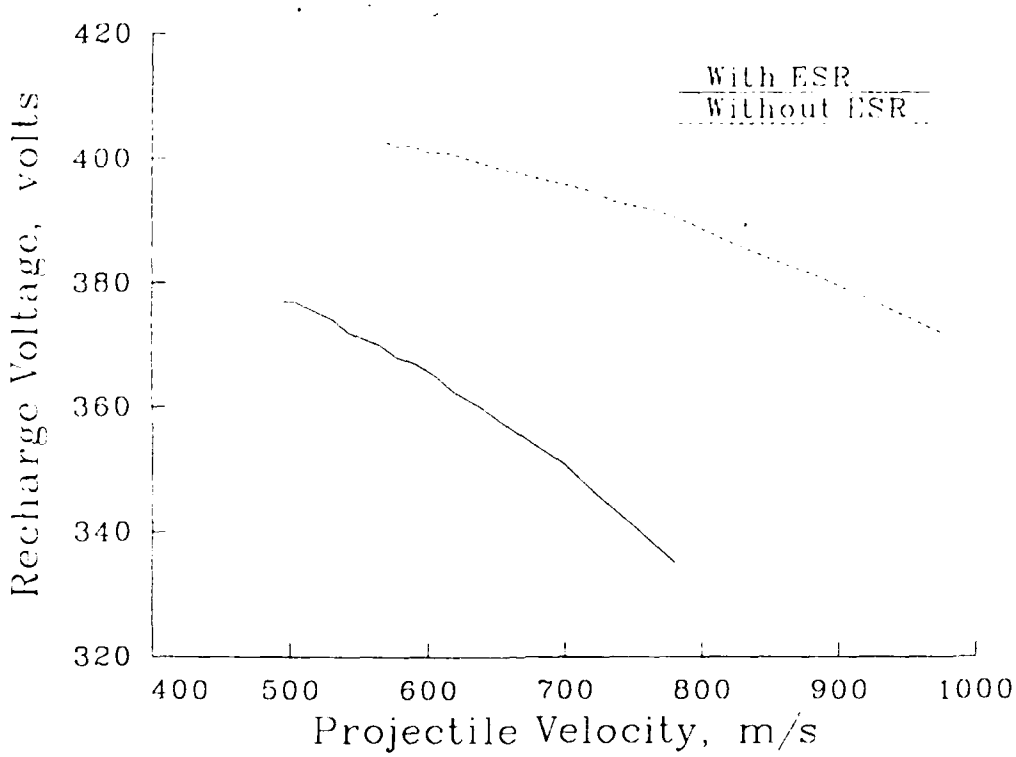

Figure 5. Predicted Recharge Voltage vs. Projectile Velocity Obtained by Varying PFN Inductance.

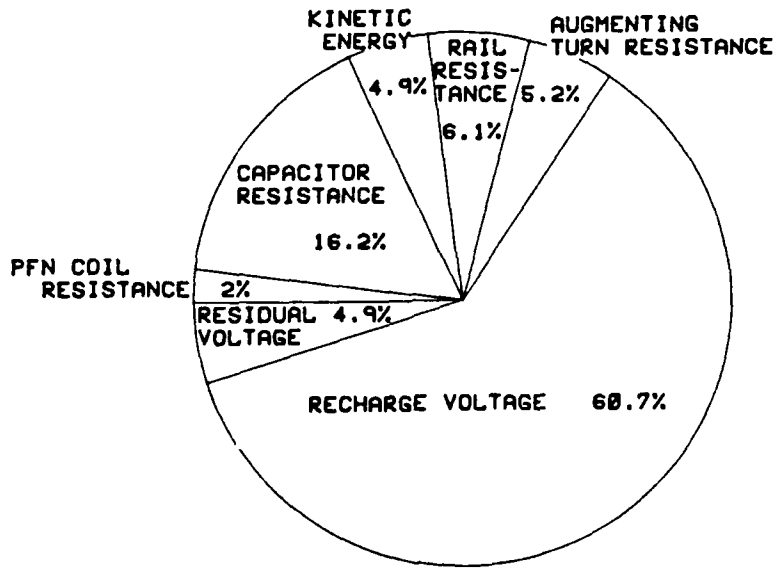

Figure 6. Energy Budget for the Power Supply Driving a 6.35 mm Square Bore Augmented Railgun.

4. FOUR MODULE EXPERIMENT

Based on the preceding circuit code simulations, the specifications for the power supply are determined and listed in Table 3.

Table 3. Module Design Parameters.

Capacitor Voltage (V)	450
Phase Capacitance (mF)	37
PFN Inductance per Module (μH)	1.0
PFN Resistance per Module (mΩ)	0.2
Peak Gun Current (kA)	146
Acceleration Time (μs)	589
Projectile Travel (mm)	230
Exit Velocity (m/s)	698

The capacitor bank is comprised of 4 modules, each supplying 25% of the total current. The SCRs and diodes selected to handle the individual module current are Westinghouse models TA20 and RA20, respectively. Recent testing indicates no capacitor voltage reversal, and, consequently, the high-current diodes were replaced with a single lower current model (1N3295). The buswork is fabricated from 6061-T6, 3-in aluminum channel and 1/4-in bar stock. The main buswork is held together with 1/4-28 tapped inserts into 1-in thick plexiglass.

The charging supply consists of two, 100 VA, 120/480 V transformers with full-wave rectification. The transformer input is controlled by a variable transformer to limit the maximum charging current. It was found that once the SCRs commutate open for a given phase, the capacitor never fully discharges to zero voltage. This residual voltage on the recently discharged phase presents an EMF, against which the next phase must discharge. Therefore, this voltage should be nulled before the negative phase discharge is initiated. This was accomplished during the polarity reversal and recharge times, with mechanical relays. Two snubber circuits (RL and RC) were added to reduce the noise created when the charging relay opens. The full schematic for operation and monitoring of the DC voltage is shown in Figure 7. When the charge relay is closed, any residual voltage on the previously discharged bank is resistively depleted through the transformer's secondary windings and the two 1 ohm resistors in series with the secondary. The two 2 ohm, 100 W resistors in series with the soft dump relay are for limiting the individual phase dump currents and consequently slowly depleting the stored capacitive energy. When the voltage has decayed to a low level (<50 V), the hard dump can be lowered to fully null any capacitor

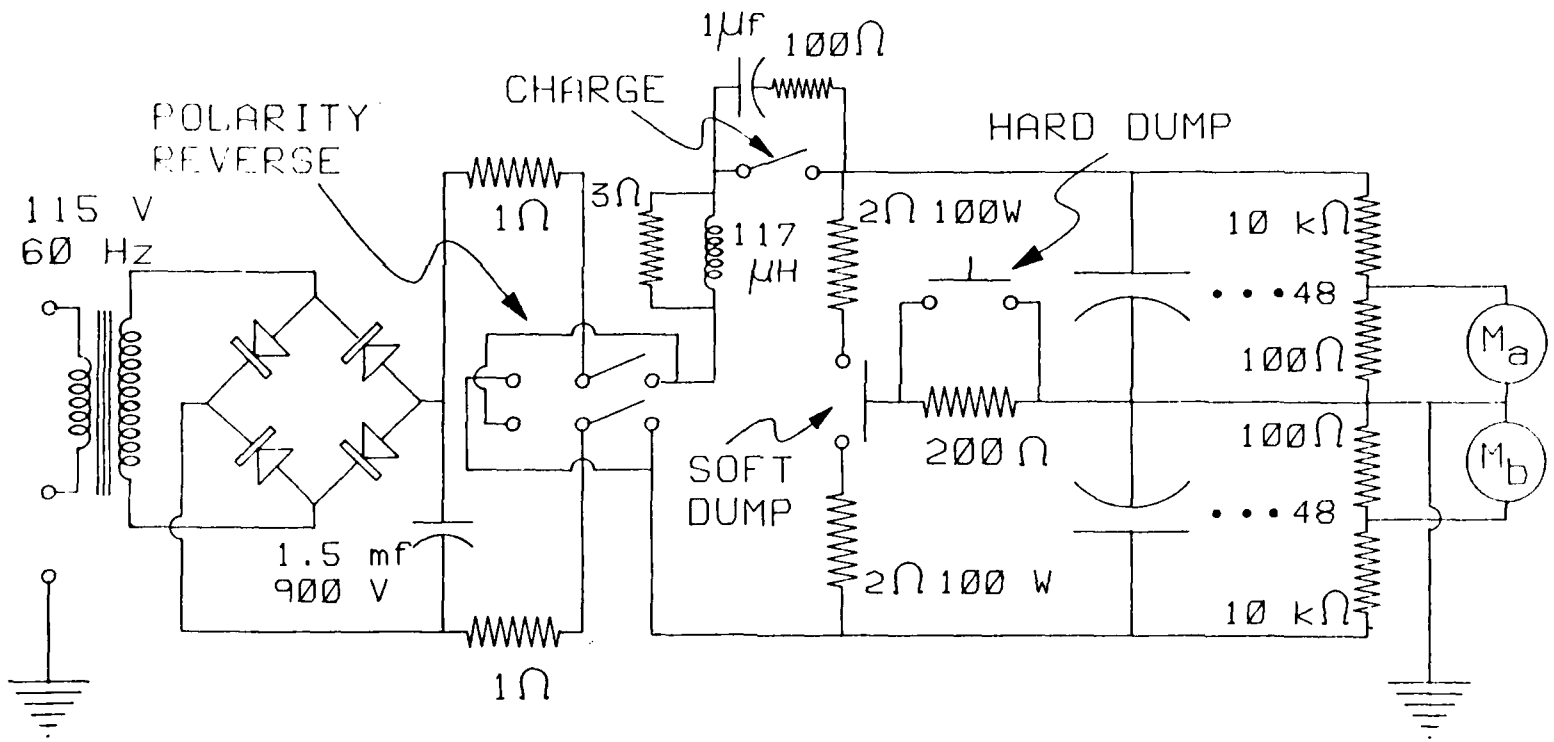

Figure 7. Schematic of Recharge Circuitry.

charge voltage. All the relays are low voltage DC controlled to reduce the amount of signal noise. The sequence of the power supply operation is as follows:

Soft Dump---------- OPEN
Hard Dump----------OPEN
Set Polarity----------POSITIVE OR NEGATIVE
Charge----------CLOSE
Charge Complete
Charge----------OPEN
Discharge

After the discharge is completed, the polarity may be reversed and the next phase recharged, or the soft dump can be lowered and the system brought down.

Initial testing used one module and various load inductances. The energy distribution for the residual voltage and recharge voltage is plotted against the PFN inductance in Figure 8. The peak voltage measured after the SCR was only 67% of the initial charge voltage with a 668 nH coil and 89% of the initial charge voltage with a 2.6 μH coil. Increasing the amount of PFN inductance increases the recharge voltage and decreases the amount of residual voltage at the expense of decreasing the peak current. If the voltage is inductively divided between the bank and the load, the resulting bank inductance is calculated to be 320 nH. The inductance calculated for the aluminum channel pair is 168 nH. This can be made lower by a more judicious placement of the capacitors and closer spacing between the buswork. The high internal bank inductance was not apparent on a previously built small module experiment which used low power semiconductors.

Four coils were constructed from 000 gage stranded wire and wound on a 3-in diameter cylindrical plexiglass form. Pulse discharge measurements and LRC bridge measurements indicate inductance and resistance values of 1.6 μH and 2.1 mΩ for each module's PFN. These values are higher than the PFN specifications listed in Table 3. With the railgun, shorted at the muzzle, serving as the electrical load, the residual energy on the discharged bank is 16% of the initial energy; the recharge energy is 32% of the initial stored energy. The peak voltage drop measured across the SCR is 15% of the initial charge voltage. A typical current trace and the circuit code prediction, both plotted against time for an initial charge voltage of 400 V, are shown in Figure 9. The predicted current pulse width underestimates the measured pulse width. Electrical characteristics for the electrolytic capacitors may differ with their charge and discharge rates as well as with the magnitude of their charge. Furthermore, actual semiconductor specifications may have to be

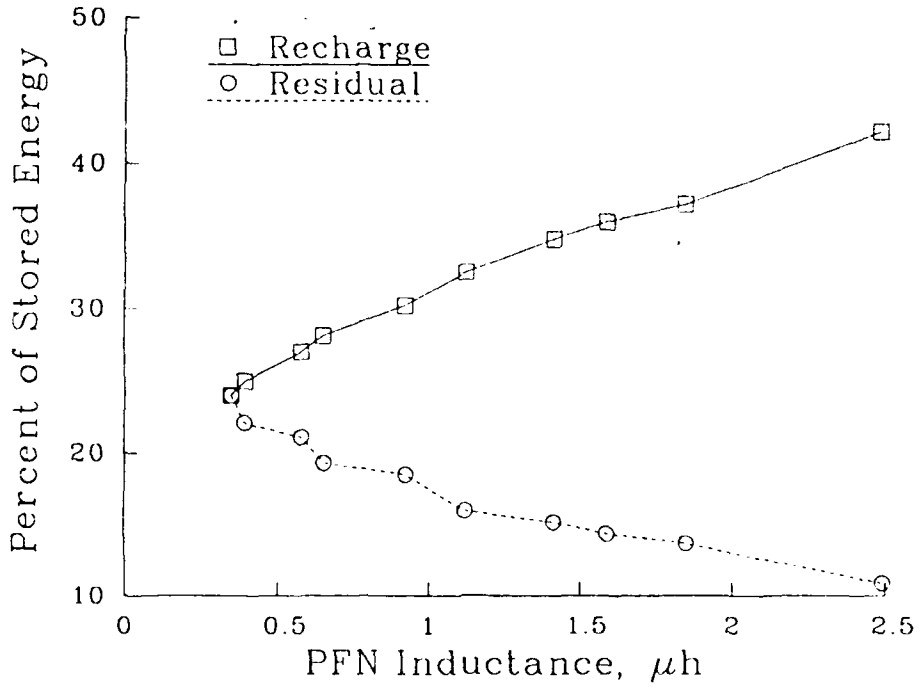

Figure 8. Energy Partitions for Residual and Recharge Capacitor Voltage vs. PFN Inductance.

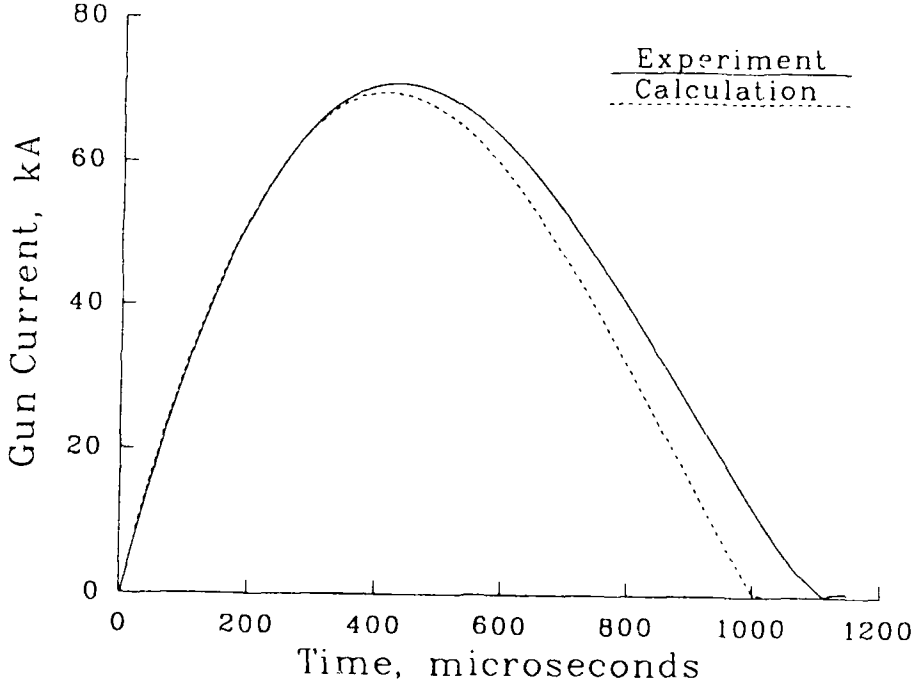

Figure 9. Measured and Predicted Current Waveforms With the Launcher Shorted at the Muzzle.

used to predict current waveforms more closely. An electrical network analysis program such as SPICE† may be required to further minimize differences between measurements and simulations.

The assembled four module capacitive power supply is visible in the background of Figure 10. To the right of the supply is a relay rack which houses the pulse and control circuitry and the 200 VA charging power supply. The 6.35 mm augmented launcher is shown in the foreground, with the wooden charge control box, which houses the relays, snubber circuits, and dump resistors, located on the floor underneath the breech end of the launcher.

The predicted current waveform when the modules drive a 2.5-g, solid aluminum armature is shown in Figure 11 (top). The initial charge voltage used in the simulation is the pulsed rating for these capacitors of 500 V. Figure 11 (bottom) also shows the resultant armature velocity plotted against time. Time-dependent models for the augmenting turn inductance and resistance, obtained from pulse discharge experiments, have been incorporated in the circuit simulation (Zielinski 1989). However, armature ohmic and frictional heating effects are ignored.

5. CONSIDERATION AS A WEAPONS SYSTEM

While the laboratory apparatus described here is certainly not ready for development into a weapon, it is worthwhile to project improvements in the various components and envision a future weapons system based on this concept. In the past, we have attempted to estimate a "system" by considering each element in the power train as an energy converter having a given conversion efficiency. Starting from the desired output of the launcher, one may work back through each element of the power train and obtain its duty cycle and capacity. Using energy and power density estimates for existing or proposed components, a crude projection may be obtained for system mass without actually performing a design study. Our present efforts are directed toward the small caliber arena, studying the possibilities for vehicle mounted, crew served, automatic weapons. Typical of conventional weapons in this class is the time-honored M2 machine gun. It is capable of firing in bursts and achieves nearly 20 kJ of projectile kinetic energy with every shot. Replacement by an electromagnetic launcher would be considered unlikely without at least a doubling in kinetic energy of the projectile and at least duplication of the burst firing rate. With heavier, faster, more lethal projectiles, a smaller burst may be acceptable, as will longer times between bursts. The starting point for envisioning the future system is then given by the set of parameters in Table 4.

---

†SPICE is a product of Micro Slim Corporation.

Figure 10. Four Module Experiment Layout.

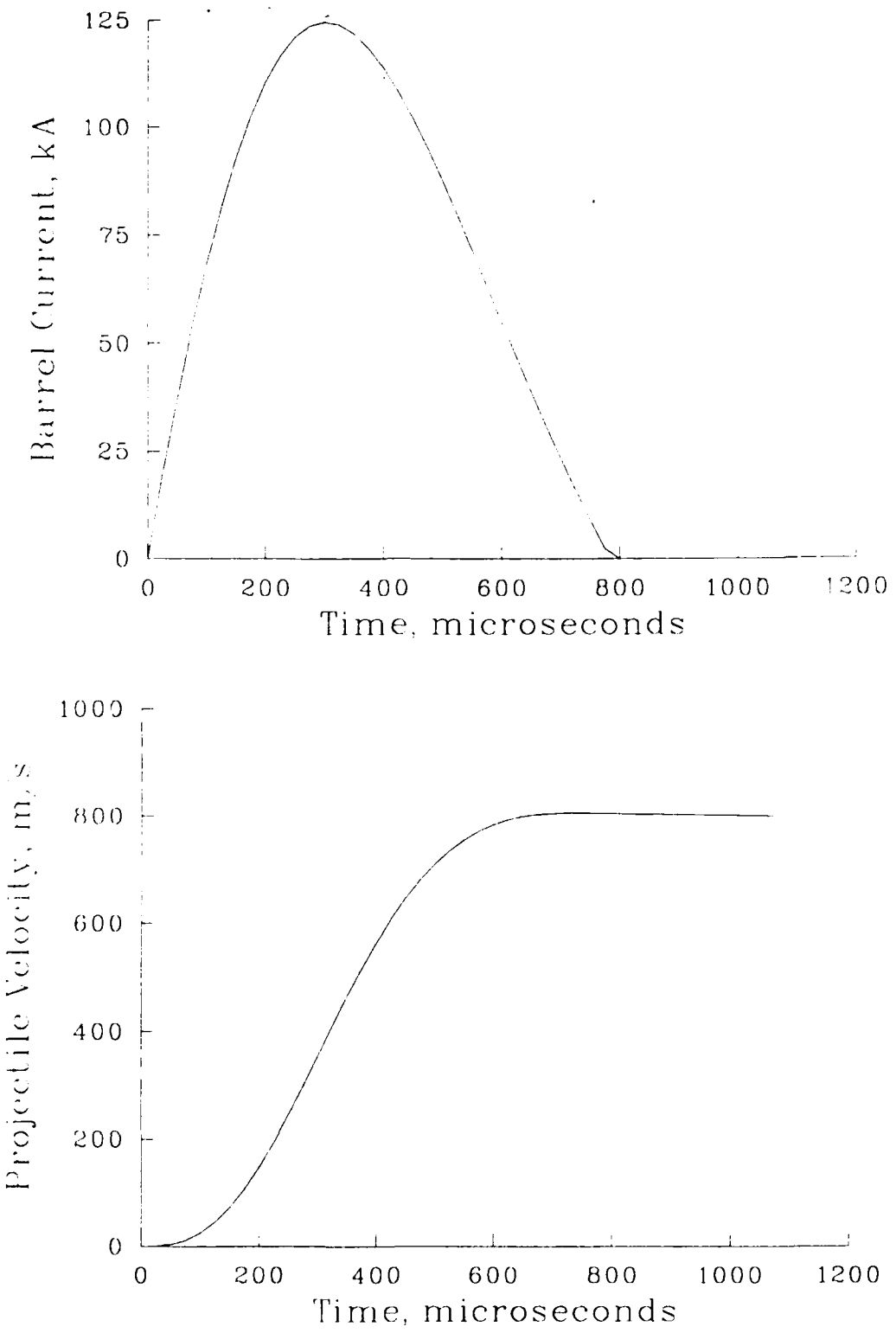

Figure 11. Predictions of Current (Top) and Velocity (Bottom) vs. Time.

Table 4. Envisioned Launcher Parameters.

Mass Stabilized Projectile Mass (g)	30
Bore (mm x mm)	14 x 14
Launch Velocity (m/s)	1634
Barrel Length (m)	1.5
Kinetic Energy (kJ)	40
Burst (rounds)	3 @ 10 Hz
Average Rate of Fire (rounds/minute)	138

Even if the gun length, projectile mass, launch velocity, and inductance gradient are fixed, one is still free within limits to select different combinations of capacitance, charge voltage, and series inductance. The constraining factor is a requirement that the current zero occur just before the projectile reaches the muzzle. Two systems are offered as examples and are outlined in Table 5.

Table 5. System A and B Parameters.

Parameters	System 'A'	System 'B'
Voltage (V)	1000	2500
Phase Capacitance (mF)	464	175
Inductance Gradient (μH/m)	0.9	0.9
Peak Current (kA)	457	376
Peak Acceleration (kgee)	320	215
Peak Bore Pressure (ksi)	70	47
Peak/Average Acceleration	3.5	2.4

The most dramatic difference in the two simulations is in peak currents. The complete current waveforms for the two systems considered are plotted in time in Figure 11. The peak acceleration drops by nearly one third as the voltage is increased from 1000 V to 2500 V. This benefit is not without a burden, however, for the energy storage requirement for System B is more than twice that for System A.

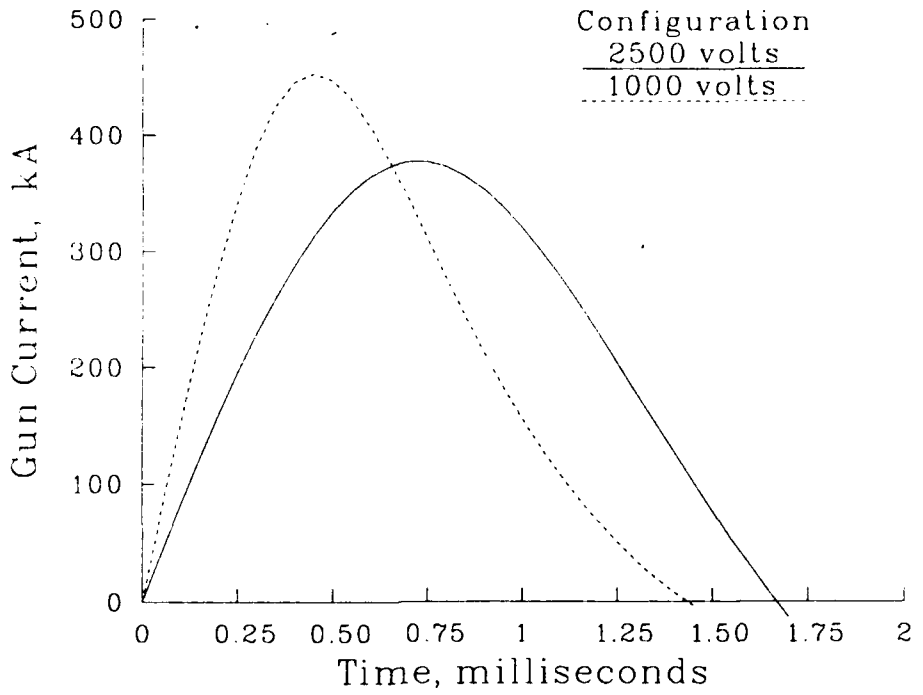

Figure 12. Predictions of Current Waveforms in Time for Two Launcher Systems.

The switchgear to deliver the requisite power to the railgun must be sized to handle the product of the capacitor bank voltage and the peak current delivered to the gun. The switchgear in the laboratory weighs about 16 kg, which, given no improvement, would set the future system requirements for switchgear at 24 and 30 kg, the lower voltage system requiring lighter gear. The storage capacity of both phases of the present laboratory bank is 30 times the kinetic energy output of the railgun. In the simulations, the low voltage case requires 232 kJ (0.464 F) in each phase of the capacitor bank while the high voltage case requires 546 kJ (0.175 F) per phase. In the laboratory device, relatively large losses are seen in the internal impedance of the capacitors, a condition which must be greatly reduced to match the simulations. Present "catalog" capacitors store energy at densities of about 0.25 kJ/kg, but proven laboratory devices store energy at densities at least ten times that value. Assuming an energy density of 2.5 kJ/kg, the total mass for the combined phases of capacitors will be 186 kg and 436 kg for Systems A and B, respectively.

A recharging device must supply a peak power of either 1.0 MW or 1.35 MW to recharge the respective systems at the 10 Hz firing rate. During a discharge, the small-capacity System A charges the second phase bank to only 50% of the original value during the shot. System B charges its second phase to 75% of the original voltage. The chargers must sustain average power levels of 265 kW and 310 kW for several minutes. Fast discharge rotating machines including recharge switchgear can be designed for peak power densities of 50 kW/kg or larger, but their duty

cycles are only a few tenths of a second per minute. The envisioned system requires a charger with a 25% duty cycle. An average power density of 1 kW/kg would appear to be an obtainable goal for an alternator with a rectifier and charging circuit. This would fix the mass of the alternator/charger at 265 kg and 310 kg for Systems A and B, respectively. A 400 hp drive engine is well matched to System A's generator while System B would require a 465 hp engine. Assuming aircraft turbine power to weight ratios, the System A drive would be about 100 kg and System B's would be about 110 kg. An autoloader/injector for either system, with 1000 rounds, is estimated at 70 kg, including a fuel tank which contains enough energy to fire all 1000 rounds. The masses of the components for both systems, from fuel to railgun, are listed in Table 6.

The mass penalty associated with reducing the acceleration is significant, but if long guns are not permitted, some consideration should be given to the larger capacity, higher voltage configurations. Integrated projectile design considerations are greatly affected by allowable acceleration limits and consequently peak barrel current.

While the mass for a small caliber weapon may at first appear excessive, the possibilities exist for even greater improvements in capacitors and solid-state devices in the future. A wide variety of vehicles exist which can carry a one ton payload.

Table 6. System Weights.

Component Weight (kg)	System 'A'	System 'B'
Fuel	60	70
Generator/Rectifier	265	310
Switch Gear	24	30
Capacitors	186	436
Autoloader	70	70
Buswork	74	50
Railgun	60	40
Total (kg)	739	1006

For comparison, the total weight of the laboratory system described in this report is 250 kg. Its kinetic output is 1/40 of the system envisioned above and relies on commercial power rather than autonomous generation. Further, it is a single-shot device without an autoloader or

injector. Clearly, the projections presented here are optimistic but are certainly within the limits of the state of the art in power supply components.

6. CONCLUSION

The original motive for this effort was to construct a laboratory device which could emulate a compulsator waveform. The power supply we have constructed in this study is inexpensive and performs this task very well, even to the point of offering very rapid pulsing at the expense of diminishing pulse amplitude. The supply has been tested on a number of loads as well as being utilized for some of our other pulse power experiments. This power supply is currently being exploited in our ongoing solid armature/projectile development program. Multishot railgun firings are planned in the very near future. Other plans include improving the present bank with a multielement PFN to allow control over the acceleration profile.

The concept of simultaneously recharging a capacitor bank during the firing of a railgun offers several attractive features. It recovers the magnetic field energy from the railgun bore. This practice improves efficiency and provides a current zero at the end of the acceleration time. The current zero is well suited to SCR switches which are able to open at the end of the discharge cycle. A current zero before projectile exit may be absolutely necessary for small projectiles which are susceptible to tip-off. Our long range plans include the consideration of this type of power conditioning for small caliber weapons applications.

INTENTIONALLY LEFT BLANK.

6. REFERENCES

Garner, J., A. Zielinski, and K. Jamison. "Design and Testing of a Mass Stabilized Projectile for a Small Caliber Electromagnetic Launcher," IEEE Transactions on Magnetics. Vol. 25, pp. 197-202, January 1989.

Powell, J. D. "Atmospheric Effects on Projectile Acceleration in the Railgun," Journal of Applied Physics. Vol. 54, pp. 7195-7197, December 1983.

Powell, J. D. Personal communication, February 1988.

SPICE, Micro Slim Corporation, 23175 LaCadena Dr., Laguna Hills, CA 92653.

Zielinski, A. E. "BRL Pulsed Power Facilities and Research Status." Paper presented at the 6th Electromagnetic Launcher Association Meeting, Eglin AFB, FL, May 1989.

INTENTIONALLY LEFT BLANK.

No of Copies	Organization
1	Office of the Secretary of Defense OUSD(A) Director, Live Fire Testing ATTN: James F. O'Bryon Washington, DC 20301-3110
2	Administrator Defense Technical Info Center ATTN: DTIC-DDA Cameron Station Alexandria, VA 22304-6145
1	HQDA (SARD-TR) WASH DC 20310-0001
1	Commander US Army Materiel Command ATTN: AMCDRA-ST 5001 Eisenhower Avenue Alexandria, VA 22333-0001
1	Commander US Army Laboratory Command ATTN: AMSLC-DL Adelphi, MD 20783-1145
2	Commander US Army, ARDEC ATTN: SMCAR-IMI-I Picatinny Arsenal, NJ 07806-5000
2	Commander US Army, ARDEC ATTN: SMCAR-TDC Picatinny Arsenal, NJ 07806-5000
1	Director Benet Weapons Laboratory US Army, ARDEC ATTN: SMCAR-CCB-TL Watervliet, NY 12189-4050
1	Commander US Army Armament, Munitions and Chemical Command ATTN: SMCAR-ESP-L Rock Island, IL 61299-5000
1	Commander US Army Aviation Systems Command ATTN: AMSAV-DACL 4300 Goodfellow Blvd. St. Louis, MO 63120-1798

No of Copies	Organization
1	Director US Army Aviation Research and Technology Activity Ames Research Center Moffett Field, CA 94035-1099
1	Commander US Army Missile Command ATTN: AMSMI-RD-CS-R (DOC) Redstone Arsenal, AL 35898-5010
1	Commander US Army Tank-Automotive Command ATTN: AMSTA-TSL (Technical Library) Warren, MI 48397-5000
1	Director US Army TRADOC Analysis Command ATTN: ATAA-SL White Sands Missile Range, NM 88002-5502
(Class. only) 1	Commandant US Army Infantry School ATTN: ATSH-CD (Security Mgr.) Fort Benning, GA 31905-5660
(Unclass. only) 1	Commandant US Army Infantry School ATTN: ATSH-CD-CSO-OR Fort Benning, GA 31905-5660
1	Air Force Armament Laboratory ATTN: AFATL/DLODL Eglin AFB, FL 32542-5000
	Aberdeen Proving Ground
2	Dir, USAMSAA ATTN: AMXSY-D AMXSY-MP, H. Cohen
1	Cdr, USATECOM ATTN: AMSTE-TD
3	Cdr, CRDEC, AMCCOM ATTN: SMCCR-RSP-A SMCCR-MU SMCCR-MSI
1	Dir, VLAMO ATTN: AMSLC-VL-D

No. of Copies	Organization
5	Commander Armament RD&E Center US Army AMCCOM ATTN: SMCAR-FSA-E (Dr. T. Gora, John Bennett) SMCAR-AEE-B (Dr. D. Downs) SMCAR-CCL-FA (H. Moore, H. Kahn) Picatinny Arsenal, NJ 07806-5000
2	Director Benet Weapons Laboratory Armament RD&E Center US Army AMCCOM ATTN: SMCAR-CCB-DS (Dr. C. A. Andrade) SMCAR-CCB-RM (Dr. Pat Vottis) Watervliet, NY 12189
1	Director DARPA ATTN: Dr. Peter Kemmey 1400 Wilson Blvd. Arlington, VA 22209
1	Commander SDIO ATTN: SDIO/IST (MAJ M. Huebschman) Washington, DC 20301-7100
4	CG, MCRDAC Code AWT ATTN: Dr. C. Vaughn Mr. C. Childers MAJ R. Jensen Mr. G. Solhand Quantico, VA 22134-5080
1	Director US Army Research Office ATTN: Dr. Michael Ciftan P. O. Box 12211 Research Triangle Park, NC 27709-2211
2	Air Force Armament Laboratory ATTN: AFATL/DLJG (Mr. Kenneth Cobb) AFATL/DLDG (Dr. T. Aden) Eglin AFB, FL 32542-5000
1	Director Brookhaven National Laboratory ATTN: Dr. J. R. Powell Bldg 129 Upton, NY 11973

No. of Copies	Organization
1	Director Lawrence Livermore National Laboratory ATTN: Dr. R. S. Hawke, L-156 P. O. Box 808 Livermore, CA 94550
3	Director Los Alamos National Laboratory ATTN: MSG 787, Mr. Max Fowler Dr. J. V. Parker Dr. William Condit Los Alamos, NM 87545
1	Sandia National I aboratory ATTN: Dr. Maynard Cowan Dept. 1220 P. O. Box 5800 Albuquerque, NM 87185
1	NASA Lewis Research Center ATTN: MS 501-7 (Lynette Zana) 2100 Brook Park Road Cleveland, OH 44135
1	Astron Research & Engineering ATTN: Dr. Charles Powars 130 Kifer Court Sunnyvale, CA 94086
2	Austin Research Associates ATTN: Dr. Millard L. Sloan Dr. William E. Drummond 1091 Rutland Drive Austin, TX 87858
3	Maxwell Laboratories ATTN: Dr. Rolf Dethlefson Dr. Michael M. Holland Dr. Mark Wilkinson 8888 Balboa Avenue San Diego, CA 92123
1	Boeing Aerospace Company ATTN: Dr. J. E. Shrader P. O. Box 3999 Seattle, WA 98134
2	GA Technologies, Inc. ATTN: Dr. Robert Bourque Dr. L. Holland P. O. Box 85608 San Diego, CA 92138

No. of Copies	Organization
2	GT Devices ATTN: Dr. Shyke Goldstein Dr. D. Tidman 5705-A General Washington Drive Alexandria, VA 22312
1	General Dynamics ATTN: Dr. Jaime Cuadros P. O. Box 2507 Pomona, CA 91766
2	Electromagnetic Research, Inc. ATTN: Dr. Henry Kolm Dr. Peter Mongeau 2 Fox Road Hudson, MA 01749
2	General Electric Company (AEPD) ATTN: Dr. William Bird Dr. Slade L. Carr R. D. #3, Plains Road Ballston Spa, NY 12020
1	General Research Corporation ATTN: Dr. William Isbell P. O. Box 6770 Santa Barbara, CA 93160-6770
2	IAP Research, Inc. ATTN: Dr. John P. Barber Mr. David P. Bauer 2763 Culver Avenue Dayton, OH 45429-3723
2	LTV Aerospace & Defense Company ATTN: MS TH-83, Dr. Michael M. Tower Dr. C. H. Haight P. O. Box 650003 Dallas, TX 75265-0003
1	Pacific-Sierra Research Corp. ATTN: Dr. Gene E. McClellan 1401 Wilson Blvd. Arlington, VA 22209
2	Physics International Company ATTN: Dr. A. L. Brooks Dr. Frank Davies 2700 Merced Street San Leandro, CA 94577
1	R&D Associates ATTN: Dr. Peter Turchi P. O. Box 9695 Marina del Rey, CA 90291
1	SAIC, Inc. ATTN: Dr. K. A. Jamison 1247-B North Eglin Parkway Shalimar, FL 32579
3	SAIC, Inc. ATTN: Dr. Jad H. Batteh Dr. G. Rolader Mr. L. Thornhill 1503 Johnson Ferry Rd., Suite 100 Marietta, GA 30062
1	System Planning Corporation ATTN: Donald E. Shaw 1500 Wilson Blvd. Arlington, VA 22209
2	Westinghouse Electric Corporation Marine Division ATTN: Dr. Dan Omry Dr. Ian R. McNab 401 East Hendy Avenue Sunnyvale, CA 94088-3499
1	Westinghouse Science and Technology Center ATTN: Dr. Bruce Swanson 1310 Beulah Road Pittsburgh, PA 15233
2	Auburn University ATTN: Dr. Raymond F. Askew Leach Nuclear Science Center Dr. E. J. Clothiaux Department of Physics Auburn University, AL 36849-3501
1	Texas Technical University Department of EE/Computer Science ATTN: Dr. M. Kristiansen Lubbock, TX 79409-4439
1	Tuskegee Institute Dept. of Mechanical Engineering ATTN: Dr. Pradosh Ray Tuskegee Institute, AL 36088
1	University of Alabama in Huntsville School of Science & Engineering ATTN: Dr. C. H. Chen Huntsville, AL 35899
1	University of Miami ATTN: Dr. Manuel A. Huerta, Physics Dept. P.O. Box 248046 Coral Gables, FL 33124

No. of Copies	Organization
1	University of Tennessee Space Institute ATTN: Dr. Dennis Keefer Tullahoma, TN 37388-8897
3	University of Texas Center for Electromechanics Balcones Research Center ATTN: Mr. William Weldon Mr. Raymond Zaworka Dr. Harry Fair 10100 Burnet Road, Bldg. 133 Austin, TX 78748
1	Dr. E. W. Sucov 1065 Lyndhurst Drive Pittsburgh, PA 15206
1	SPARTA Inc. ATTN: Jeffery Kezerian 9455 Towne Centre Drive San Diego, CA 92121-1964
	Supercon Inc. ATTN: Charles Renaud 830 Boston Turnpike Road Shrewsbury, MA 01545
	Aberdeen Proving Ground
1	Cdr, USATECOM ATTN: AMSTE-SI-F